Bioinspiration &
Biomimetics

PURPOSE-LED
PUBLISHING™

PAPER · **OPEN ACCESS**

Substrate-dependent friction and climbing performance in a flying snake

To cite this article: Jonas Scherer *et al* 2026 *Bioinspir. Biomim.* **21** 066007

View the article online for updates and enhancements.

You may also like

- Impact-induced adhesion degradation in gecko-inspired fibrillar adhesive units
Ru-Guo Ji, Yue-Yu Yuan, Xiao-Feng Liu et al.
- Cooperative propulsion in multi-scale V-shaped fish schools
Jinghan Lin, Mingming Wang, Jing Sun et al.
- Bioinspired trajectory tracking control of an underactuated robotic fish using prescribed-time and prescribed-performance control
Xinqi Wang, Ming Wang, Xinyang Liu et al.

This content was downloaded from IP address 73.171.44.254 on 21/11/2026 at 22:22

Bioinspiration & Biomimetics

Check for updates

OPEN ACCESS

RECEIVED
4 June 2026

REVISED
18 September 2026

ACCEPTED FOR PUBLICATION
29 October 2026

PUBLISHED
18 November 2026

Original content from this work may be used under the terms of the Creative Commons Attribution 4.0 licence.

Any further distribution of this work must maintain attribution to the author(s) and the title of the work, journal citation and DOI.

PAPER

Substrate-dependent friction and climbing performance in a flying snake

Jonas Scherer[1], **Hodjat Pendar**[2] and **John J Socha**[2,*]

[1] Department of Biology, Bielefeld University, Bielefeld, Germany
[2] Department of Mechanical Engineering, Virginia Tech, Blacksburg, VA, United States of America
[*] Author to whom any correspondence should be addressed.

E-mail: jjsocha@vt.edu

Keywords: frictional anisotropy, snake locomotion, bioinspired robotics

Supplementary material for this article is available online

Abstract

Locomotion in limbless animals depends on friction between the body and substrate. In snakes, the skin-substrate interface can generate frictional anisotropy, lowering resistance during forward motion while increasing resistance during backward or transverse motion. These properties have inspired models and robots that rely on directional friction, yet empirical measurements remain limited across species and substrates. We measured static and dynamic coefficients of friction in a flying snake, *Chrysopelea paradisi*, using an inclined-plane method on four artificial substrates and one natural substrate, poplar bark. We quantified passive friction in forward, backward, and transverse directions in anesthetized snakes and estimated critical slip angles and whole-animal effective slip resistance in awake snakes, and examined climbing kinematics across platform inclinations. Across substrates, forward friction was lower than backward and transverse friction, and static friction differed strongly among substrates, with bark producing the highest resistance. In some trials on bark, ventral scales engaged asperities and intermittently caught the substrate, producing elevated apparent resistance not readily described as conventional friction. Awake snakes climbed progressively steeper inclines on high-purchase substrates and climbed vertically on bark. As purchase decreased on smoother substrates or steeper inclines, snakes increased lateral excursions, locomotion became less regular, and animals transitioned to an impulsive push gait with irregular anchors and intermittent slip. We also used a planar simulation to test how the transverse/forward friction ratio, μ_T/μ_F, influences net displacement. Increasing μ_T/μ_F increased simulated displacement, but ratios near the biologically measured range produced limited displacement relative to higher-anisotropy conditions. Together, these results show that snake skin-substrate interactions depend not only on directional friction coefficients, but also on discrete mechanical interaction with asperities. For bioinspired locomotor systems, effective anisotropic friction may require multiscale surface structure, intermittent anchoring, and modulation of body-substrate contact rather than simple Coulomb friction alone.

1. Introduction

For terrestrial animals, forward movement over a substrate requires friction for creating propulsive forces (Alexander 2003, Biewener and Patek 2018). Limbed animals employ friction at discrete contacts of the foot, where friction prevents slip and allows muscular forces to be redirected into ground reaction forces with a forward component. As long as static frictional limits are not exceeded, propulsion is governed primarily by limb kinematics and force orientation rather than by the magnitude of friction itself.

In limbless animals like snakes, forward movement is produced through a continuous body-substrate contact, where friction both limits and shapes the direction and magnitude of propulsive

© 2026 The Author(s). Published by IOP Publishing Ltd

forces (Hu and Shelley 2012). Snakes employ multiple forms of locomotion including lateral undulation, concertina, rectilinear, and sidewinding, the use of which depends on factors including species and environment (Jayne 2020). In many of these forms and their variants, a major contrast with limbed locomotion is the use of sliding friction. In lateral undulation, the most common mode of locomotion in snakes, waves of muscular bending help to create propulsive forces that push off asperities of the substrate, enabling the body to slide forward along the body's path (Moon and Gans 1998). In this type of locomotion, net forward translation is greatly aided, or perhaps even only possible, by a frictional anisotropy between the skin and the substrate (Hu *et al* 2009). Specifically, resistance to sliding is smaller anteriorly than it is posteriorly or laterally, a frictional imbalance that biases ground reaction forces in the forward direction. Direction-dependent friction forces thus determine how effectively normal forces generated by axial bending are redirected into propulsive forces.

The frictional properties of a snake result from scale microstructure and scale overlap along the body, and how these morphological features interact with the substrate (Wu *et al* 2020, Rieser *et al* 2021). In addition, snakes can modulate their engagement with the substrate using behaviors like body lifting (Hu *et al* 2009) or erection of ventral scales to increase the effective angle of attack of scale edges (Marvi and Hu 2012, Marvi *et al* 2016). Overall, understanding friction between skin and substrate is central to understanding how snakes move in terrestrial environments.

The importance of friction for snake locomotion is further reflected in models that aim to explain the links between force production and kinematics. Current mathematical frameworks often parameterize the ratio between transverse (i.e. in the lateral direction) and longitudinal (i.e. in the axial direction) friction, using a wide range of theoretical values from negligible to extremely high (e.g. Alben 2013, 2019, 2022, Mei *et al* 2024). The models demonstrate that the efficacy of a specific locomotor mode is sensitive to the friction ratio. For instance, when the friction ratio is low and close to one (isotropy), lateral undulation yields negligible net forward displacement, whereas sidewinding remains possible. Conversely, higher friction ratios significantly enhance the performance of lateral undulation.

Despite these theoretical insights, empirical measurements of friction ratios in snakes remain sparse, having been characterized in only a small number of species. Early macroscopic observations by Gray and Lissmann (1950) showed that whole animals sliding on wood or metal surfaces exhibited direction-dependent frictional resistance. Modern detailed friction measurements have been carried out on colubrids including *Lampropeltis triangulum* (Hu *et al* 2009), *Lampropeltis getula* (Baum *et al* 2014), *Pantherophis guttatus* (Marvi and Hu 2012, Wu *et al* 2020), and *Spalerosophis diadema* (Wu *et al* 2020); boids including *Corallus hortulanus* (Berthé *et al* 2009), pythonids including *Python regius* (Abdel-Aal *et al* 2012), and *Aspidites ramsayi* (Wu *et al* 2020); viperids including *Vipera aspis, Sistrurus miliarius*, and *Bitis arietans* (Wu *et al* 2020); and elapids including *Naja atra* (Wu *et al* 2020). These species represent only a small fraction of 3,000+ extant species and a subset of the broad ecological strategies used by snakes.

Because friction is determined by the interaction of the object of interest and the surface, actual friction coefficients and their directional ratios depend on the experimental substrate examined. Most studies have used artificial substrates for reproducibility and utility of comparison, and also because studies of locomotion are often conducted on these substrates. For example, the studies mentioned previously examined surfaces such as glass, acrylic, polymer films, and micropatterned polymers. Natural terrestrial surfaces like soil or grass have not been investigated, impeding understanding of snake locomotion in an ecological context.

Arboreal habitats impose additional constraints on locomotion in snakes because climbing requires resisting gravity while generating adequate purchase on bark or other vegetative surfaces. Arboreal locomotion also differs from terrestrial because the weight of the snake provides little to no contribution to the normal force that determines friction (Jayne 2020). In this study, we investigate friction in an arboreal snake, the flying snake *Chrysopelea paradisi*. We chose this species because as a group, flying snakes experience perhaps the largest range of locomotor challenges in the arboreal environment (Socha 2011). Like other arboreal species, it must climb up and down on substrates that include trunks, branches, leaves and vines. But additionally, flying snakes are capable of jumping, a locomotor behavior found in only a few groups of snakes (Graham and Socha 2021, 2023). The J-loop jump, the snake's most energetic mode of jumping, involves both sliding over a surface to form a pre-jump posture, and then anchoring the rear body statically while the anterior body accelerates during the jump (Socha 2006). This impulsive locomotor behavior can be used to cross small gaps or to begin a glide and cross larger expanses. In either case, the trajectory terminates when the snake lands on vegetation or the ground, a process that can produce relatively high impact forces on the skin (Dellinger *et al* 2023).

In this study, we (i) quantify direction-dependent static and dynamic coefficients of friction of *Chrysopelea paradisi* across substrates spanning three orders of magnitude in roughness, and (ii) relate these frictional properties to climbing kinematics

and performance across platform inclinations. We examined artificial substrates commonly used in arboreal snake locomotion studies (e.g. Astley and Jayne 2009, Byrnes and Jayne 2012, Crotty and Jayne 2015, Graham and Socha 2021, 2023) as well as natural bark, used in gliding flight studies (Socha 2002, 2006, Socha *et al* 2005, 2010). We predicted that both transverse and longitudinally backward friction would exceed forward friction, with the strongest effects on rough substrates. We further predicted that decreasing purchase (smoother substrates and/or steeper inclines) would elicit gait transitions consistent with anchor-based locomotion predicted by existing models.

2. Materials and methods

We measured static and dynamic coefficients of friction for anesthetized *Chrysopelea paradisi* on five substrates using an inclined-plane method and quantified substrate roughness using digital microscopy. We then recorded climbing trials of awake snakes on the same substrates across platform inclinations to relate frictional properties to performance and kinematics. All procedures were approved by the Virginia Tech Institutional Animal Care and Use Committee (IACUC 16–154) and were conducted in accordance with institutional animal-care guidelines.

2.1. Animals

Five *Chrysopelea paradisi* (snout-vent length: 64.4–95.9 cm; mass: 44.0–117.5 g) were used in this study. Snakes were housed individually at 25°C–27°C and 45%–55% relative humidity with shelters and climbing structures, fed thawed mice weekly, and were not tested within 48 h of feeding.

2.2. Friction measurements

We used an inclined-plane method (figure 1) to determine friction coefficients, following previous studies (e.g. Hu *et al* 2009, Marvi and Hu 2012). This technique relies on a geometric relationship: for an object on an incline, the angle of the incline (θ) at the onset of sliding determines the static coefficient of friction (μ_s). Specifically,

$$\mu_s = \tan\theta \tag{1}$$

μ_s equals tan(θ), where θ is the incline angle relative to horizontal. We used this relation to determine μ_s in three directions relative to the snake's body axis (forward, backward and transverse) on five substrates. For trials in which snakes slid continuously, we estimated the dynamic (or kinetic) coefficient of friction (μ_k) from displacement over time at a fixed incline angle using the standard constant-acceleration relation for motion down an incline. Specifically,

$$\mu_k = \tan\theta - \frac{2x}{gt^2\cos\theta} \tag{2}$$

where x is displacement, t is time, and g is gravitational acceleration (9.81 m s^{-2}). This equation assumes that the snake remains in contact with the surface without rolling, and the friction force remains constant.

The inclined plane consisted of a plywood board (1.83 × 1.83 m) mounted on an aluminum frame (80/20 Inc., Columbia City, Indiana, U.S.) and connected to a winch-and-pulley system used to change the angle manually. An acrylic sheet (polymethyl methacrylate, 1.7 mm thick) was hot-glued onto the plywood to serve as the base substrate for all test substrates. Interchangeable fiberboard panels (1.52 × 1.22 m; 3 mm thick) carried each substrate: acrylic (Thrifty White Panel Board acrylic coating, The Home Depot, Atlanta, Georgia, U.S.), duct tape (Duct Tape Pro Strength, Scotch, St. Paul, Minnesota, U.S.), seam tape (Ram Board Seam Tape, Valencia, California, U.S.), gaffer's tape (GaffTac Gaffer Tape, Rosco, Stamford, Connecticut, U.S.), and poplar tree bark (Bark House, Highland Craftsmen, Inc., Spruce Pine, North Carolina, U.S.). The tapes were applied to each surface in abutting lengthwise strips, carefully applied such that there was no overlap between strips. Their orientation was top-to-bottom, meaning that the tape edges were parallel to the sides of the board. The bark panels were purchased as flat panels, custom-created by soaking and then flattening. Fourteen such panels were mounted to a fiberboard using screws from the bottom side to avoid damaging the surface. The bark panels exhibited natural spatial variation in texture. To reduce bias from this heterogeneity, we selected panels with similar gross structure, randomized their placement when constructing the surface, and treat the bark condition as a heterogeneous natural substrate rather than as a uniform material.

A video camera (Hero4 Silver, GoPro Inc., San Mateo, California, U.S) was used to record all trials at 30 frames per second. The camera was attached to an L-shaped aluminum frame such that it faced downward and recorded a top view of the snake.

In trials to determine μ_s, the snake was placed in the middle of the board with the body oriented in three directions relative to the downslope direction: forward, backward, and transverse (figure 1). Starting from the level position, the incline angle was slowly increased using the hand crank of the winch; when the snake began sliding, the angular increase was immediately terminated. Trials to determine μ_k were similar except that the snake was allowed to slide until it reached the bottom of the board. In those trials, the

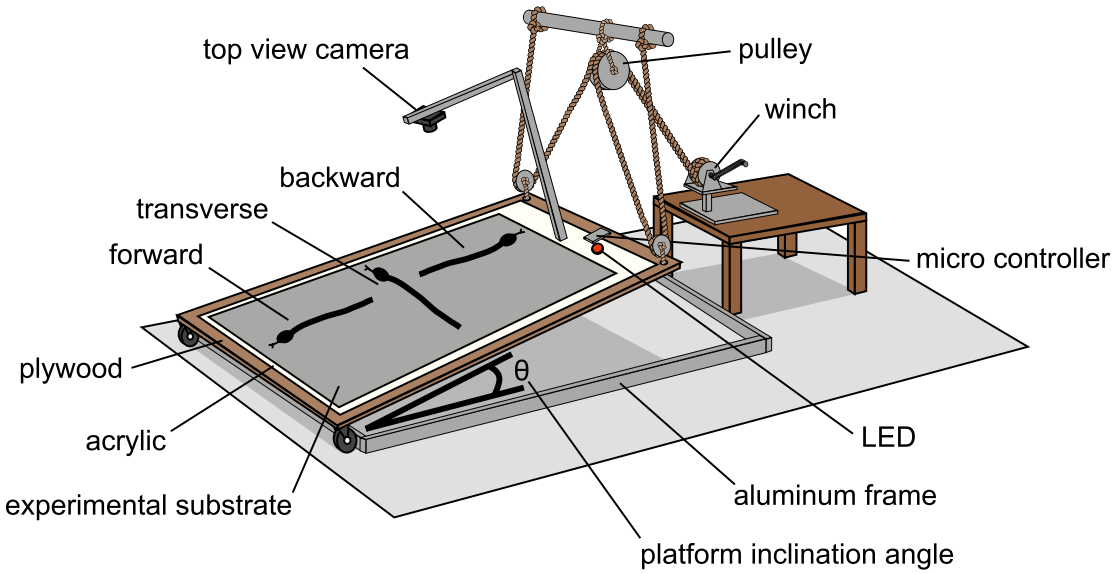


Figure 1. Experimental apparatus used for the inclined-plane method used to quantify coefficients of friction. The snake icons are shown to demonstrate their relative positioning for measurements of forward, backward and transverse coefficients. In actual trials, the snake was placed in the middle of the board. Objects are not depicted to scale.

sideways configuration was not tested because preliminary trials demonstrated that the snake would roll rather than slide. Transverse static trials were included only when the body slid downslope without visible rolling at the onset of motion. Trials in which the snake rolled were excluded from analysis.

Incline angle was measured in two ways, using a digital inclinometer (18" Digital Angle Protractor, Denali, Redmond, Washington, U.S.) and an angle-measuring gyroscope module (GY-521 with InvenSense MPU-6050 six-axis gyro and accelerometer MEMS MotionTracking Device chip, San José, California, U.S.). The module was wired to a microcontroller programmed to measure the angle at a rate of 5 Hz and output the average at 1 Hz. The microcontroller also had a red flashing LED that was used to synchronize the angular output to the recorded video post-hoc. We used the mean of both measures unless the video recording indicated a lag between slip and cessation, in which case we used only the gyroscope-derived angle.

Snakes were anesthetized using fumes of isoflurane. The snake's head was placed into a plastic bag with a piece of cotton soaked with 1.0–1.5 ml 99% isoflurane, adjusted by snake mass. The snake was removed when muscle tone indicated a suitable depth of anesthesia. The snake's heartbeat and respiration were monitored throughout the procedure. To minimize applications of anesthesia, all trials for an individual snake on a surface were done in the same session. Snakes were then given a minimum of 48 h of rest before the next surface was tested.

For awake snakes, we increased incline angle until a stationary snake slipped during a climbing attempt. Because posture was not standardized and included a mix of both lateral and posterior body contacts, these trials were not treated as conventional directional coefficients of friction. Instead, we report the critical slip angle and the corresponding effective slip resistance, calculated as $\tan(\theta)$, as whole-animal measures during climbing.

Five snakes were used in anesthetized friction measurements, although not every individual was tested on every substrate; four snakes, excluding ID 95, were used for awake slip and climbing trials.

2.3. Climbing performance

In addition to the anesthetized trials, we recorded climbing trials of awake snakes on the same substrates. In these trials, we incrementally increased the incline angle until snakes failed to make forward progress. Success was defined as the head reaching the top edge. Motivation to climb was provided by artificial leaves attached to the top edge and, when needed, we gently prodded the snake's tail by hand or snake-handling hook. Such prodding was used only to initiate movement; we cannot rule out an effect of motivation on trial-to-trial behavior, but kinematic summaries were calculated from forward-moving bouts and did not include frames during direct experimenter contact. Using MATLAB, we quantified kinematics by tracking the head and centroid positions from overhead video for all substrates except bark, which lacked sufficient contrast. The centroid of the snake was estimated as the geometric centroid of the visible body outline in the image plane, not as a mass-weighted center of mass. We computed uphill velocity, body-axis orientation (centroid-to-head vector)

and the directions of head and centroid velocity vectors relative to the uphill direction.

2.4. Surface roughness

We quantified substrate topography of each substrate using a digital microscope (KH-7700, Hirox USA, Hackensack, New Jersey, U.S.) to obtain pseudo in-focus images and 3D surface reconstructions. For each substrate, we sampled three positions; for bark, we sampled both a relatively smooth and a relatively rough panel. Bark samples were positioned to ensure that the diagonal sampling always recorded a ridge valley and elevation peaks. From diagonal height profiles, we calculated standard roughness metrics at each magnification: R_a, the arithmetic mean deviation roughness, R_z, the ten-point mean roughness, and R_q, the root-mean-square-deviation roughness.

2.5. Statistics

Statistical analyses were performed in MATLAB using linear mixed-effects models. To avoid treating repeated trials from the same individual as independent biological replicates, passive friction measurements were first averaged within each snake, substrate, direction, and friction type; these animal-level means were used for the primary analyses. Static and dynamic friction were analyzed separately because transverse dynamic friction was not measured. Coefficients of friction were log-transformed before modeling. For each friction type, we first fit a model including substrate, direction, and their interaction, with snake ID as a random intercept. When the interaction was not supported, we interpreted an additive model including substrate and direction, also with snake ID as a random intercept. Raw-scale and trial-level models were run as sensitivity analyses. Trials on poplar bark in which the snake slid completely (with visible scale engagement) were excluded and summarized separately. Frictional anisotropy ratios were calculated within individual snakes from animal-level means and then summarized across snakes.

Awake slip trials were analyzed separately from anesthetized friction trials. Effective slip resistance was calculated as tan(critical slip angle, θ), log-transformed, and analyzed with substrate as a fixed effect and snake identity as a random intercept. Poplar bark was excluded from this model because snakes did not slip on that substrate. Maximum successful platform inclination angle was analyzed from one value per snake per substrate using a mixed-effects model, with substrate as a fixed effect and snake ID as a random intercept; the single 130° bark overhang trial was exploratory and therefore excluded.

Uphill velocity, head movement direction, and centroid movement direction were analyzed using mixed-effects models with substrate, platform inclination, and their interaction as fixed effects and snake ID as a random intercept. Bark was included in the uphill-velocity analysis but excluded from head- and centroid-direction analyses because those kinematic variables were not measured on bark. When the substrate-by-inclination interaction was not supported, an additive model was used for interpretation. A sensitivity analysis for uphill velocity was also run after excluding high-velocity points identified by a median absolute deviation criterion. Model-level P values were calculated using Satterthwaite denominator degrees of freedom. Values are reported as mean ± s.d. unless stated otherwise.

2.6. Simulation of planar locomotion

To evaluate the consequences of the measured frictional anisotropy ratios in a simplified locomotor framework, we implemented a planar snake-locomotion model with prescribed lateral undulation and anisotropic Coulomb-like friction. This model follows the general structure of previously published models of snake locomotion on flat substrates (Hu *et al* 2009, Alben 2013, Zhang *et al* 2021). The simulated snake had non-dimensional length 1 and a prescribed traveling wave of curvature, κ, as given in (Zhang *et al* 2021),

$$K(s,t) = \alpha \cos\left[2\pi\ (s+t)\right],$$

where s is normalized arclength from tail to head, t is time, and $\alpha = 7$ (Zhang *et al* 2021). The centerline of the body was reconstructed by integrating curvature to obtain local body orientation and then integrating the tangent vector along the body. The model solved for the translational and rotational motion of the body generated by the prescribed shape change under anisotropic friction. The non-dimensionalized friction forces along the body were calculated using the friction model presented in (Hu *et al* 2009, Alben 2013, Zhang *et al* 2021):

$$\begin{aligned}\boldsymbol{f}(s,t) = &-\mu_{\mathrm{T}}\left(\hat{\boldsymbol{v}}\cdot\hat{\boldsymbol{e}}_{\mathrm{T}}\right)\hat{\boldsymbol{e}}_{\mathrm{T}} \\ &-\left[\mu_{\mathrm{F}}H\left(\hat{\boldsymbol{v}}\cdot\hat{\boldsymbol{e}}_{\mathrm{F}}\right)+\mu_{\mathrm{B}}\left(1-H\left(\hat{\boldsymbol{v}}\cdot\hat{\boldsymbol{e}}_{\mathrm{F}}\right)\right)\right]\left(\hat{\boldsymbol{v}}\cdot\hat{\boldsymbol{e}}_{\mathrm{F}}\right)\hat{\boldsymbol{e}}_{\mathrm{F}}\end{aligned}$$

where $\hat{\boldsymbol{v}}(s,t)$ is the normalized local velocity of the body point, $\hat{\boldsymbol{e}}_{\mathrm{F}}$ and $\hat{\boldsymbol{e}}_{\mathrm{T}}$ are the tangential and transverse (normal to the body) unit vectors, and H denotes the Heaviside function.

The forward friction coefficient was held constant at $\mu_{\mathrm{F}} = 1$, and the transverse friction coefficient was varied from $\mu_{\mathrm{T}} = 1$–12, providing a simulated anisotropy ratio $\mu_{\mathrm{T}}/\mu_{\mathrm{F}}$ from 1 to 12. This ratio corresponds most closely to the transverse/forward friction ratio used in planar models of lateral undulation, rather than to backward/forward friction. For each value of $\mu_{\mathrm{T}}/\mu_{\mathrm{F}}$, the equations of motion were integrated from $t = 0$–20. To minimize effects of initial transients, net performance was quantified as centroid displacement between $t = 10$ and $t = 20$, divided by the elapsed time. The simulation was not intended to model other real components of the experimental snake movements, which include vertical climbing,

asperity-catching, or active normal-force redistribution; instead, it was used to test how much displacement is predicted by a planar anisotropic-friction model when friction ratios are in the range measured experimentally and beyond.

3. Results

3.1. Surface analysis

Across artificial substrates, acrylic and seam tape were the smoothest; duct tape and gaffer's tape were rougher (figure 2, table 1). The relative roughness of duct tape and gaffer's tape depended on magnification, with duct tape slightly rougher at 140*x*, but gaffer's tape rougher at 560*x*. Poplar bark was two to three orders of magnitude rougher than the artificial substrates.

The images also reveal qualitative features of interest. The seam tape includes randomly arranged fibers and a connecting matrix that form a wavy surface. The duct tape has parallel rows of elevations connected by smoother regions. The gaffer's tape includes thin fibers arranged in a square weave.

3.2. Friction of anesthetized snakes

Static friction coefficients differed strongly among substrates and directions in animal-level mixed-effects models (figure 3(A); tables 2 and 5). The surface-by-direction interaction was not statistically supported ($F_{8,24.46} = 1.51$, $P = 0.204$), so the additive model was used for interpretation. In that model, static friction differed significantly among substrates ($F_{4,32.74} = 26.28$, $P < 0.001$) and directions ($F_{2,32.26} = 13.07$, $P = < 0.001$). Forward static friction was lower than backward friction, but transverse friction did not differ from backward friction. Compared to acrylic, static friction coefficients were higher on duct tape, gaffer's tape, and poplar bark; seam tape did not differ from acrylic. Static friction coefficients were lowest on acrylic and seam tape, higher on duct tape and gaffer's tape, and highest on bark, but there was not a pattern of monotonic increase across the artificial substrates. Directional anisotropy ratios calculated within individual snakes are reported in table 3.

Backward and transverse static friction were generally higher than forward static friction, but the relative magnitude of backward and transverse friction varied among substrates. However, in some backward trials on bark, the trial culminated in complete sliding of the snake down the plane. In such trials, we noticed that ventral scales engaged bark asperities and intermittently caught the substrate (figure 4). These occurrences were identified visually by the experimenter during the trials and thus are treated qualitatively; one such event was recorded by video as an exemplar and shown in figure 4. Values from trials with visible engagement are shown only for comparison and should not be interpreted as conventional coefficients of friction (mean apparent resistance = 1.41 ± 0.57, $N = 3$ snakes, $n = 11$ trials; table 2).

Dynamic friction coefficients showed a similar directional pattern. The surface-by-direction interaction was not statistically supported for dynamic friction ($F_{4,15.05} = 0.55$, $P = 0.703$), but the additive model indicated significant effects of substrate ($F_{4,20.32} = 7.65$, $P < 0.001$) and direction ($F_{1,19.14} = 15.12$, $P < 0.001$). Forward dynamic friction was lower than backward dynamic friction. Dynamic friction also differed among substrates, with poplar bark producing the clearest increase relative to acrylic. Dynamic coefficients were generally lower than static coefficients (table 2).

3.3. Friction of awake snakes

Critical slip angle and effective slip resistance during awake slip trials were analyzed separately from anesthetized friction trials. Effective slip resistance differed strongly among the artificial substrates ($F_{3,7.79} = 65.21$, $P < 0.001$), increasing from acrylic to seam tape, duct tape, and gaffer's tape (tables 4 and 5). Relative to the mean of backward and transverse static friction in anesthetized snakes, awake effective resistance was approximately 0.8x on acrylic, 1.3x on seam tape, 1.4x on duct tape, and 1.7x on gaffer's tape. Awake snakes did not slip on vertical bark, preventing estimation of an effective slip resistance.

3.4. Climbing performance of awake snakes

Climbing performance in awake snakes changed with platform inclination angle and substrate (figures 5 and 6, Supplementary Movies 1, 2). Mixed-effects analysis of the velocity data (figure 5(A)), with snake identity as a random intercept, showed that uphill velocity decreased as platform inclination angle increased ($\beta = -0.44$ cm s^{-1} deg^{-1}, $P < 0.001$). The relationship did not differ clearly among substrates; the substrate *x* platform-inclination-angle interaction was not statistically supported ($F_{4,102.55} = 1.88$, $P = 0.120$), so the additive model was used for interpretation. The velocity data show that snakes generally moved more slowly at steeper inclines. Maximum climbable platform inclination angle increased across substrates (figures 5(B)–(F), table 4) and differed strongly among substrates ($F_{4,12} = 394.65$, $P < 0.001$): snakes climbed progressively steeper inclines on the artificial substrates, and all snakes climbed vertically on bark. Because bark performance was capped at the vertical test angle, the bark value represents a minimum estimate of maximum performance rather than a finite performance limit.

When purchase was high (rough substrates and/or shallow inclines), snakes used regular lateral undulation with relatively uniform wavelength and amplitude. As purchase decreased, locomotion became less regular and snakes increased lateral

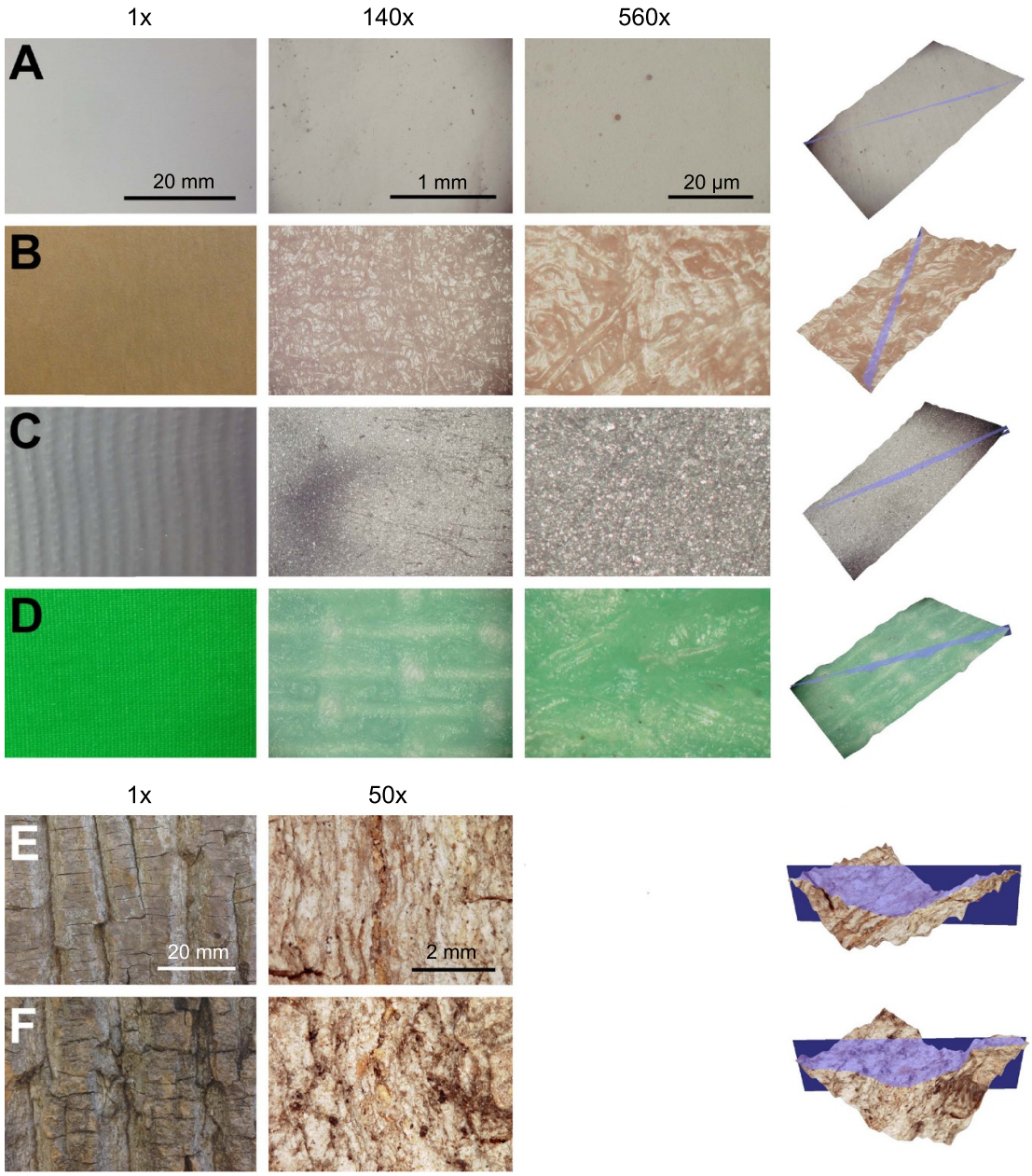


Figure 2. Surface features of the substrates used in this study. The top group of images represent macrostructural (1x), mesostructural (140x), microstructural (560x), and topographic 3D images of artificial substrates acrylic (A), seam tape (B), duct tape (C), and gaffer's tape (D); the bottom group are natural substrates smooth poplar bark (E), and rough poplar bark (F). For A through D, scale bars are 20 mm (1x), 1 mm (140x), and 20 μm (560x). For E and F, scale bars are 20 mm (1x) and 2 mm (50x). The topographic 3D images were generated using the 140x and 50x magnification images, respectively.

excursions (figure 6). At low purchase, snakes adopted an irregular anchor-based pushing gait. These movements involved intermittent slipping, and discrete, impulsive forward advances generated by straightening or reorienting the anterior body bends (also see Supplemental figure S1). Mixed-effects analyses of the movement-direction data (figure 7) showed that both head and centroid velocity vectors deviated increasingly from the uphill direction as platform inclination angle increased. Head movement direction increased by approximately 1.05 degrees per 1 degree increase in platform inclination ($P < 0.001$), and centroid movement direction increased by approximately 1.00 degrees per 1 degree increase in platform inclination ($P < 0.001$). Evidence for substrate-specific slopes was weak after accounting for repeated observations from individual snakes. Qualitatively, slipping appeared more frequently on smoother substrates and at steeper platform inclinations. By contrast, movement on

Table 1. Results of roughness measurements on the five surfaces. R_a, R_z, and R_q represent the arithmetic mean deviation roughness, the ten-point mean roughness, and the root mean square deviation roughness, respectively. Values are mean ± standard deviation. For each row, standard deviations represent variation among six diagonal height profiles from three fields of view (two diagonals per field). The microscope magnification used for each measurement is also indicated.

Surface	Magnification	R_a (μm)	R_z (μm)	R_q (μm)
Acrylic	140x	4.5 ± 5	21.1 ± 14	5.7 ± 5.1
	560x	1.9 ± 0.5	8.1 ± 1.4	2.3 ± 0.5
Seam tape	140x	9.2 ± 3.7	51.4 ± 27.3	11.6 ± 5
	560x	5.8 ± 1.8	30.2 ± 7.5	7.1 ± 2.1
Duct tape	140x	20.3 ± 8.1	94.7 ± 31.1	24.5 ± 9.1
	560x	12.4 ± 3.6	43.5 ± 9.2	14 ± 3.9
Gaffer's tape	140x	17.4 ± 4.5	93.7 ± 32.7	22.3 ± 6.3
	560x	17.7 ± 12.5	70.5 ± 34.5	20.2 ± 12.8
Smooth bark	50x	1275 ± 301	4737 ± 1242	1461 ± 324
Rough bark	50x	1755 ± 449	7045 ± 1793	2092 ± 587

bark was more continuous, demonstrating a body-following pattern similar to that exhibited by most snake species during (non-slipping) lateral undulation on terrestrial substrates.

3.5. Simulation of planar locomotion

The planar simulation showed that net displacement increased strongly with frictional anisotropy ratio. When transverse and forward friction were equal ($\mu_T/\mu_F = 1$), the prescribed lateral-undulation wave produced little net displacement of the snake's centroid (figure 8). Increasing μ_T/μ_F increased net displacement, with the largest gains occurring as the ratio increased from nearly isotropic values toward moderately anisotropic values. The experimentally measured static transverse/forward anisotropy ratios generally fell near the lower end of this simulated range.

4. Discussion

4.1. Frictional anisotropy and substrate dependence

Across substrates, *C. paradisi* exhibited lower forward friction than backward and transverse friction, consistent with prior measurements of snake skin friction (Berthé *et al* 2009, Hu *et al* 2009, Abdel-Aal *et al* 2012, Marvi and Hu 2012, Baum *et al* 2014, Wu *et al* 2020). Friction also depended strongly on substrate, with duct tape, gaffer's tape, and poplar bark producing higher static friction than acrylic. However, friction did not increase monotonically with measured roughness. Seam tape did not produce higher friction than acrylic despite its higher measured roughness, suggesting that roughness metrics alone were insufficient to predict friction. Other properties may also have contributed, including adhesion, compliance, fiber orientation, surface contamination, and the geometry of asperities relative to scale edges.

These results are consistent with friction and frictional anisotropy arising from ventral microstructure, scale overlap, and mechanical interaction with substrate texture. Bark provided the clearest case of substrate-specific mechanical engagement: it had the largest backward/forward static-friction ratio and was the only substrate on which visible scale catching was observed. Because such catching reflects discrete engagement of scale edges with asperities, the resulting resistance should be viewed as a combined effect of friction and geometric interlocking, rather than as a classical coefficient of friction.

4.2. Gait transitions with declining purchase

Climbing kinematics varied systematically with substrate and platform inclination. Mixed-effects analyses of the kinematic data showed that uphill velocity decreased as platform inclination angle increased, whereas head and centroid movement vectors became increasingly oblique to the uphill direction. These results indicate that snakes moved more slowly and used more laterally directed movements as climbing became more difficult. When push points were abundant and platform inclination was low, snakes used lateral undulation, which can minimize repeated static frictional events because much of the body slides continuously. As platform inclination increased and/or substrate purchase decreased, snakes increased lateral excursions, a behavior that may reflect searching for discrete asperities. Below a purchase threshold, snakes transitioned to an irregular anchor-based pushing gait that differs from canonical concertina locomotion (Gray 1946, Gans 1970, Jayne 1988, 2020, Jayne and Davis 1991, Marvi and Hu 2012): anchors were irregular, static and sliding regions shifted rapidly along the body, and slipping occurred often. This gait resembles anchor-based patterns predicted by planar locomotion models in which low transverse friction favors intermittent anchoring, but our observations also indicate an important role for three-dimensional

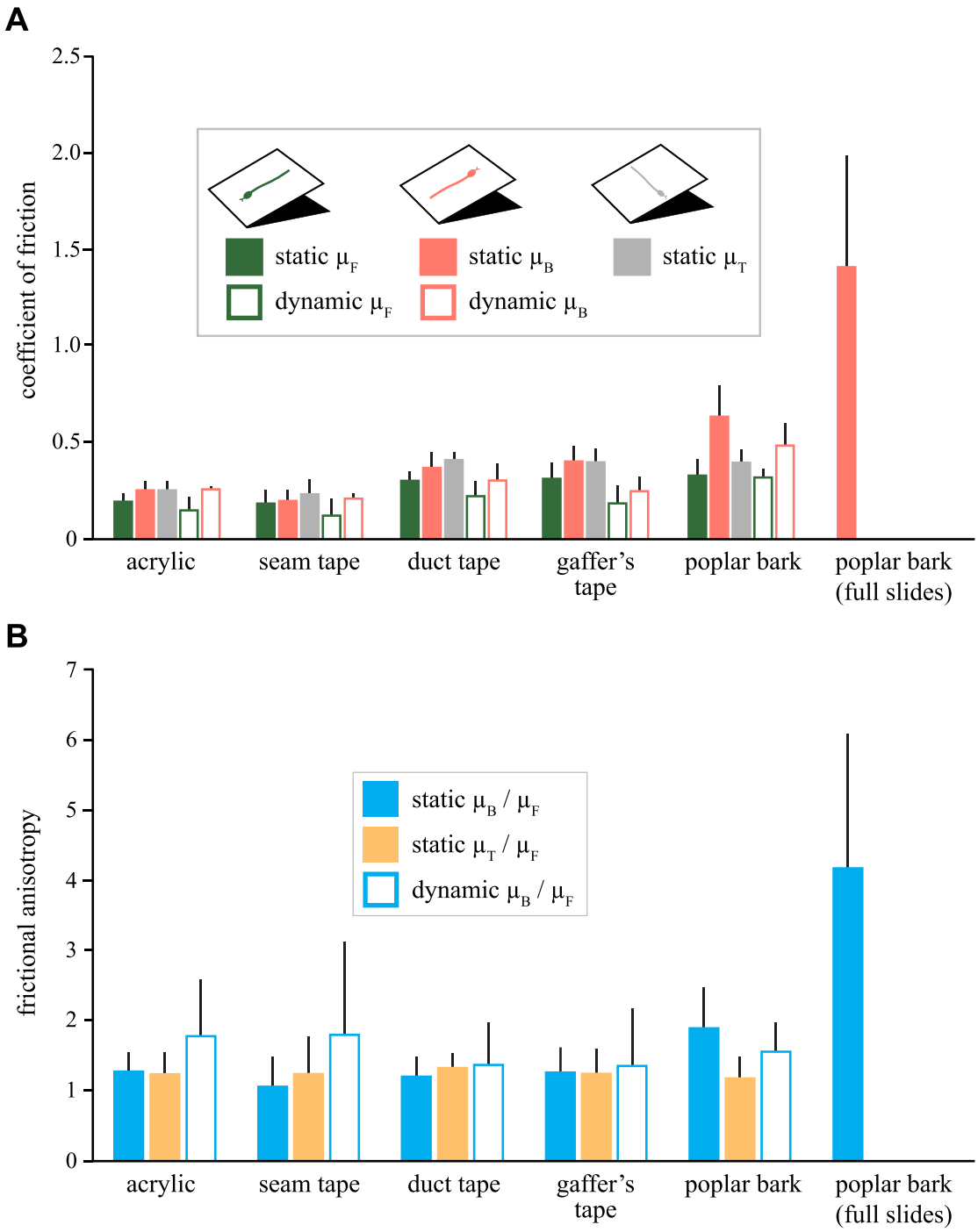


Figure 3. Coefficients of friction for anesthetized *Chrysopelea paradisi*. (A) Comparison of coefficients of friction across surfaces. F = forward, B = backward, T = transverse. Static and dynamic coefficients are represented in solid and empty bars, respectively. Transverse dynamic friction was not quantified. Summary coefficients are provided in table 2; statistical results are provided in table 5. Trials in which the snake slid down the board completely (rather than slip and arrest, as with all other data) are indicated as 'full slides' and should not be interpreted as conventional coefficients. (B) Ratios of friction coefficients across surfaces. Anisotropies calculated from friction values in static state (filled) and dynamic state (outlined) are shown. Numeric values are provided in table 3. For both (A) and (B), error bars represent standard deviation.

mechanisms (body lifting, keel engagement, and scale catching) that are not captured by planar models.

On bark, all snakes climbed vertically, and movement appeared more continuous and lateral undulation-like than on smoother substrates. Combined with the high backward resistance on bark and the occurrence of visible catching, these results suggest that rough bark provides both abundant asperities for transverse force application and opportunities for scale-edge engagement on steep inclines. Although incline angles beyond 90° were not systematically tested, one snake continued to climb in an exploratory trial as the board was tilted beyond vertical, up to an angle of 130°. This anecdotal observation should be viewed cautiously because it involved only

Table 2. Results of static and dynamic coefficient of friction measurements on the five surfaces in all tested directions. Values are mean ± standard deviation. F = forward, B = backward, and T = transverse, as defined in figure 1. N = number of snakes; n = number of trials. Bark full-slide events are excluded from conventional coefficient-of-friction values, and are provided as descriptive apparent resistance values.

	Static					
Surface	μ_F	N/n	μB	N/n	μT	N/n
Acrylic	0.20 ± 0.026	3/9	0.26 ± 0.036	3/9	0.25 ± 0.051	3/9
Seam tape	0.19 ± 0.056	3/9	0.20 ± 0.044	3/9	0.24 ± 0.065	3/9
Duct tape	0.31 ± 0.039	3/9	0.38 ± 0.065	3/9	0.42 ± 0.026	3/9
Gaffer's tape	0.32 ± 0.069	3/9	0.41 ± 0.066	3/9	0.41 ± 0.060	2/5
Poplar bark	0.34 ± 0.069	4/15	0.64 ± 0.143	3/9	0.40 ± 0.053	1/5
Poplar bark (full-slide)	N/A	N/A	1.41 ± 0.573	3/11	N/A	N/A

	Dynamic			
Surface	μ_F	N/n	μB	N/n
Acrylic	0.14 ± 0.066	2/3	0.25 ± 0.018	2/3
Seam tape	0.11 ± 0.085	3/6	0.20 ± 0.024	3/6
Duct tape	0.22 ± 0.075	3/5	0.29 ± 0.089	3/5
Gaffer's tape	0.18 ± 0.093	3/5	0.24 ± 0.081	3/6
Poplar bark	0.31 ± 0.044	3/6	0.48 ± 0.121	3/9
Poplar bark (full-slide)	N/A	N/A	N/A	N/A

Table 3. Calculated static and dynamic coefficient of friction anisotropies for the five surfaces in all tested directions. Values are mean ± standard deviation. F = forward, B = backward, and T = transverse, as defined in figure 1. N = number of snakes. Bark full-slide events are excluded from conventional coefficient-of-friction values, and are provided as descriptive apparent resistance values.

	Static				Dynamic	
Surface	μ_B/μ_F	N	μ_T/μ_F	N	μ_B/μ_F	N
Acrylic	1.29 ± 0.08	3	1.26 ± 0.21	3	1.72 ± 0.38	2
Seam tape	1.10 ± 0.11	3	1.30 ± 0.27	3	2.52 ± 1.45	3
Duct tape	1.22 ± 0.16	3	1.36 ± 0.14	3	1.40 ± 0.17	3
Gaffer's tape	1.30 ± 0.18	3	1.18 ± 0.04	2	1.36 ± 0.33	3
Poplar bark	2.02 ± 0.56	3	1.58	1	1.67 ± 0.26	2
Poplar bark (full-slide)	4.66 ± 2.73	3	N/A	N/A	N/A	N/A

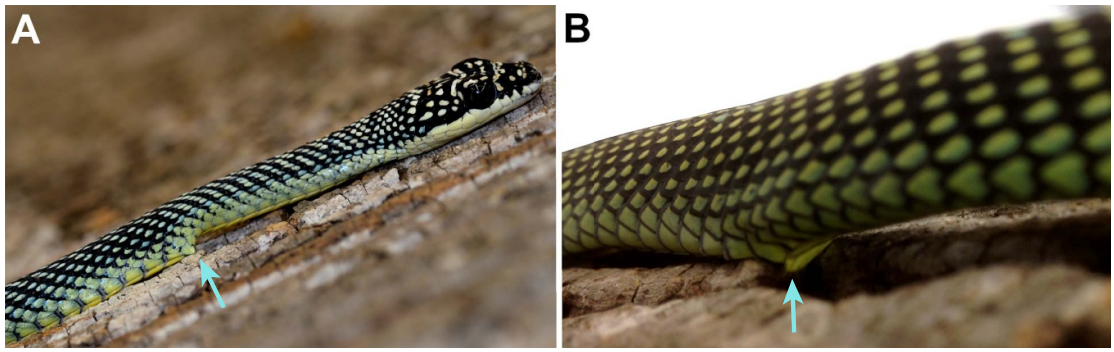


Figure 4. Ventral scale catching of an anesthetized *Chrysopelea paradisi* on poplar bark. The images show catches near the head (A) and in the midbody (B) in different trials, indicated with blue arrows. Each example shows passive elevation of the body anterior to the catch.

one individual, but it suggests that climbing performance by *Chrysopelea* on rough bark can be high. Future studies using controlled three-dimensional kinematics and force measurements could test whether rib mobility and/or scale-edge engagement (Jayne *et al* 2015, Jayne 2020) contribute to this performance.

The strong performance advantage on bark indicates that substrate texture can be a key determinant of arboreal locomotor capacity in flying snakes, suggesting multiple ecomechanical hypotheses. If smoother bark reduces purchase and increases time or risk during ascent, snakes might preferentially select rough-barked trees when climbing. Conversely,

Table 4. Awake-snake climbing performance and effective slip resistance on five substrates. Maximum successful platform inclination angle was measured during climbing-success trials. Effective slip resistance was measured in separate awake-slip trials and calculated as tan(θ); therefore, these values are not the tangent of the maximum successful climbing angle. Values are mean ± s.d. For poplar bark, effective slip resistance is not reported because the snakes did not slip; one individual was tested in an exploratory overhang trial and climbed to 130°.

Surface	Maximum successful platform inclination angle (°)	N/n	Effective slip resistance	N/n	Critical slip angle from mean effective resistance (°)
Acrylic	4.9 ± 1.00	4/4	0.21 ± 0.025	4/12	11.8
Seam tape	10.3 ± 1.82	4/4	0.28 ± 0.047	3/9	15.6
Duct tape	20.8 ± 3.44	4/4	0.54 ± 0.118	4/12	28.6
Gaffer's tape	27.6 ± 7.42	4/4	0.71 ± 0.094	4/12	35.3
Poplar bark	90	4/4	N/A	—	N/A

Table 5. Summary of statistical analyses. Passive friction, awake effective slip resistance, climbing performance, and climbing kinematics were analyzed using mixed-effects models with snake ID as a random intercept. Passive friction models used animal-level means calculated within each snake x substrate x direction x friction-type combination. For static and dynamic friction, the full model tested the substrate x direction interaction; when this interaction was not supported, additive models were used to interpret substrate and direction effects. Awake effective slip resistance and maximum successful platform inclination angle were analyzed with surface-only models because substrate was the only fixed effect. Uphill velocity, head movement direction, and centroid movement direction were analyzed using models with substrate, platform inclination angle, and their interaction as fixed effects. Trials on bark that resulted in full slides with visible scale engagement were excluded and summarized separately. *P* values are from model-level *F* tests using Satterthwaite denominator degrees of freedom.

Metric	Model type	Term	df	*F*	*P*
Anaesthetized:					
Static friction	Full	Surface *x* direction	8, 24.46	1.51	0.204
	Additive	Surface	4, 32.74	26.28	**<0.001**
	Additive	Direction	2, 32.26	13.07	**<0.001**
Dynamic friction	Full	Surface x direction	4, 15.05	0.55	0.703
	Additive	Surface	4, 20.32	7.65	**<0.001**
	Additive	Direction	1, 19.14	15.12	**<0.001**
Awake:					
Effective slip resistance	Surface only	Surface	3, 7.79	65.21	**<0.001**
Maximum successful platform inclination angle	Surface only	Surface	4, 12	394.65	**<0.001**
Uphill velocity	Full	Surface *x* platform inclination angle	4, 102.55	1.88	0.120
	Additive	Surface	4, 106.09	18.09	**<0.001**
	Additive	Platform inclination angle	1, 104.96	42.66	**<0.001**
Head movement direction	Full	Surface *x* platform inclination angle	3, 84	2.84	0.043
Centroid movement direction	Full	Surface *x* platform inclination angle	3, 82.83	0.91	0.442
	Additive	Surface	3, 85.18	25.94	**<0.001**
	Additive	Platform inclination angle	1, 85.48	57.66	**<0.001**

jumping or gliding may be preferentially employed as an escape strategy on smooth-barked trees where rapid vertical ascent is compromised. However, it is unknown if and how flying snakes jump from a vertical substrate like a tree trunk. Other arboreal vertebrate gliders, such as colugos and *Draco* lizards, use body rotations and leg-powered push-off during vertical take-off from a trunk (Byrnes *et al* 2008, Panyutina *et al* 2015, Khandelwal *et al* 2023, McWhirter-Hall *et al* 2026). Without legs, flying snakes must use another strategy, using the body both for grip and to produce an impulsive acceleration. Or, they may reserve jumping for more horizontally-oriented substrates. These hypotheses could be tested with field or laboratory observations of perch choice and escape behavior across tree species and substrate textures.

4.3. Implications for modeling snake locomotion

The results of this study reinforce current understanding of friction anisotropy in snakes and provide empirical constraints for models of limbless locomotion on textured substrates. Two factors that strongly affect locomotor performance are frictional anisotropy and the spatial redistribution of normal forces along the body, often described as friction modulation (Hu *et al* 2009, Alben 2013, Zhang *et al* 2021). Our mixed-effects analyses indicate that

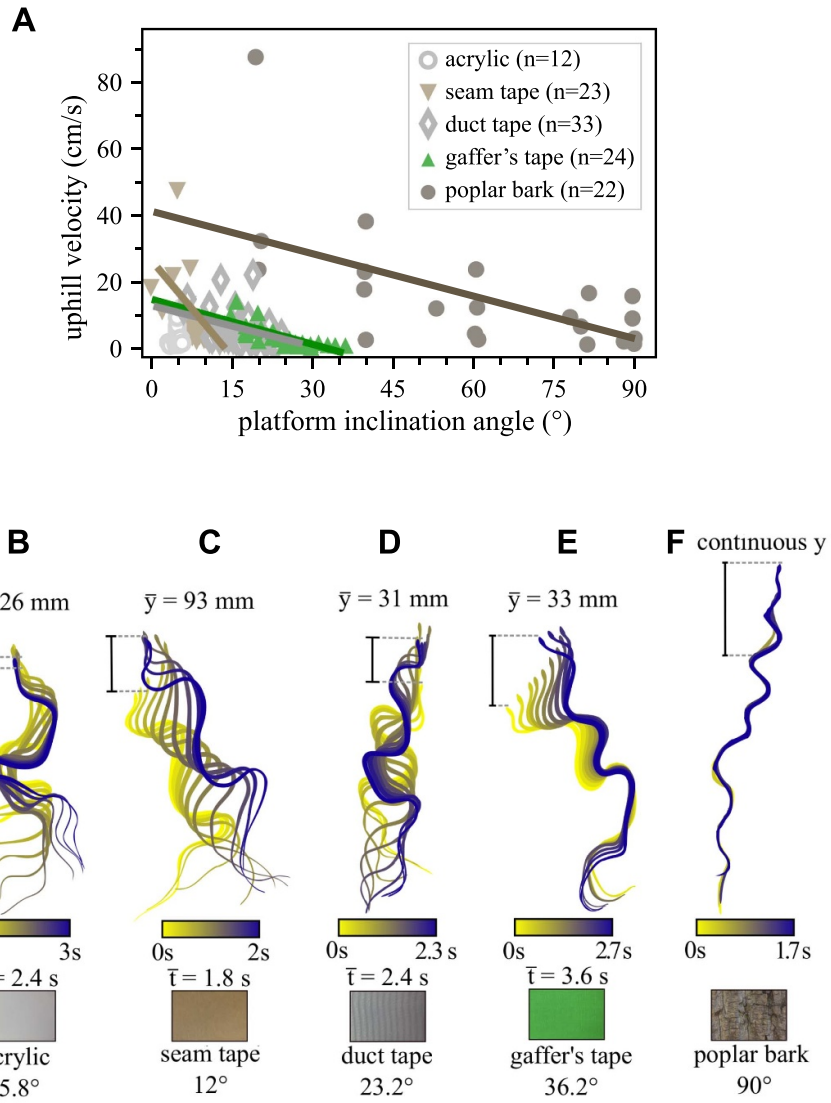


Figure 5. Differences in climbing performance of awake snakes across substrates and platform inclinations. (A) Uphill velocity plotted against platform inclination for each substrate. One data point for every awake trial is displayed. Data points were acquired by averaging uphill velocity over the whole time course of each trial. Regression statistics are provided in table S4; the line is not displayed for acrylic because it was not statistically significant. Average uphill velocity for acrylic, seam tape, duct tape, gaffer's tape, and bark are displayed. (B–F) Representative movement patterns at the steepest successful platform inclination angle on each substrate. Shown are movement patterns of a representative *Chrysopelea paradisi* ($m = 44$ g, svl = 72.5 cm) at the snake's steepest successful climb (platform inclination angle) on each substrate. The bark figure (F) represents continuous movement up a 90° slope. The movement patterns on acrylic (B) and seam tape (C) show impulsive movements of the anterior body. Y bar indicates the net forward travel of the head averaged over the whole trial. Video data are available in supplementary movie S1.

substrate altered overall friction magnitude and that friction direction had a consistent effect across substrates, whereas substrate-by-direction interactions were not strongly supported. Thus, substrate-specific friction magnitude and general directional anisotropy should be treated separately in models, rather than assuming that each substrate produces a distinct anisotropy pattern.

Previous modeling studies show that lateral undulation is strongly influenced by the ratio of transverse to forward friction. Under assumptions of isotropic friction and a uniform, constant normal force distribution between the body and the ground, models predict negligible net displacement after each locomotor cycle (Alben 2013, 2022, Zhang *et al* 2021). Increasing the transverse/forward friction anisotropy enhances net displacement, but ratios near 1–2 still produce limited forward motion relative to higher-anisotropy conditions. For example, Zhang and colleagues (Zhang *et al* 2021) shows that when the friction anisotropy ratio is between 1 and 2, the net displacement remains below 20% of the body wavelength.

These comparisons support the conclusion that passive frictional anisotropy alone is unlikely to explain the climbing performance observed in awake snakes. More broadly, they suggest that frictional anisotropy alone cannot account for planar

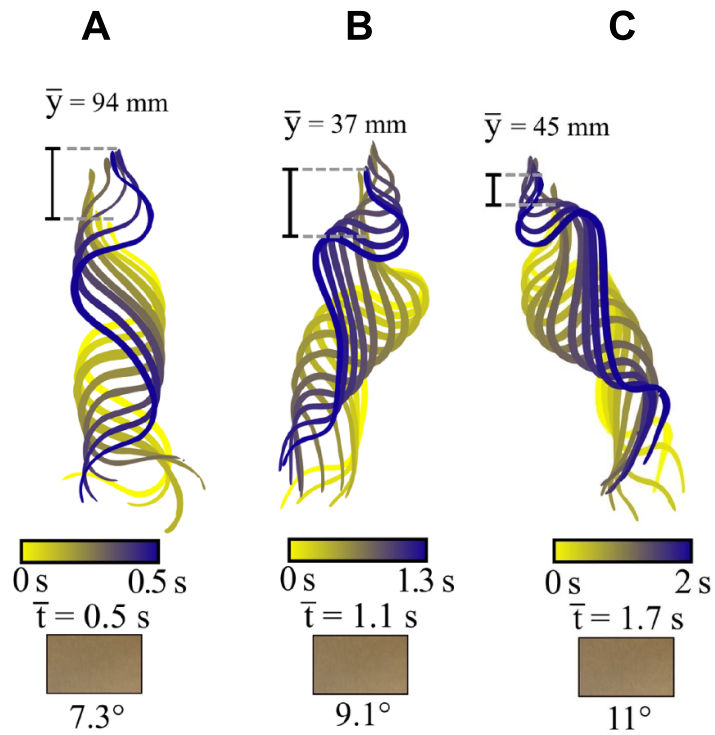


Figure 6. Climbing movement is more wave-like on lower slopes. Shown are movement patterns of representative movements of one *Chrysopelea paradisi* ($m = 56.5$ g, svl = 73.5 cm) on seam tape with flat (A), intermediate (B) and steep (C) slopes, relative to the maximal climbing success angle. All figures represent single forward strikes. The movement patterns on 9° (B) and 11° (C) show impulsive push locomotion. Video data are available in supplementary movie 2.

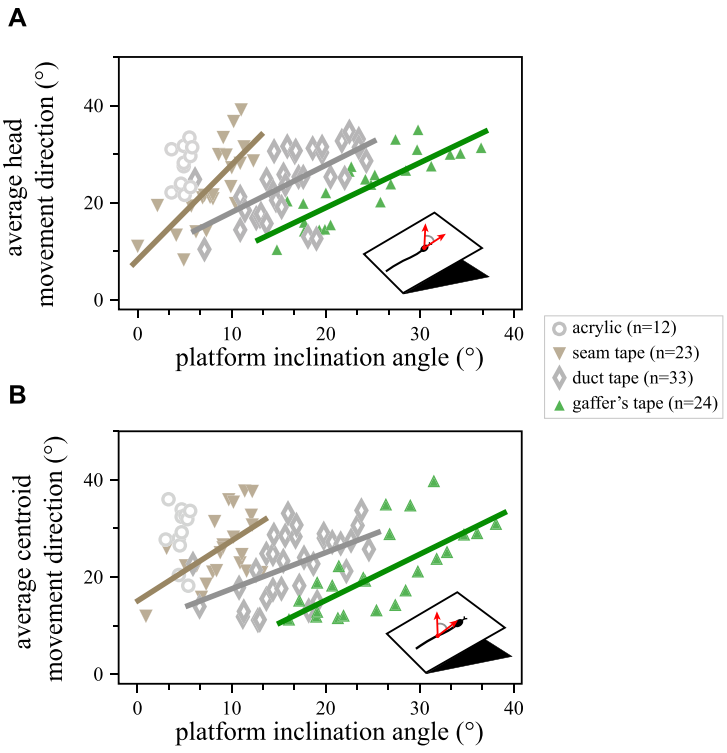


Figure 7. Changes in movement direction with platform inclination. Head and centroid do not move straight up the plane on steep angles. Shown is average movement vector direction of the head (A) and average movement vector direction of the centroid (B) separated by surface. The head and centroid velocity vectors are defined by the vector connecting the head (or centroid) in one frame with the head (or centroid) in the next frame. One data point per awake trial is displayed. All angles are calculated relative to the vector pointing straight up the plane. Lines indicate least-squares regressions; acrylic was not significant. Regression statistics are provided in tables S5 and S6; the line is not displayed for acrylic because it was not statistically significant. These analyses were not conducted for bark due to insufficient contrast between the snake and the surface.

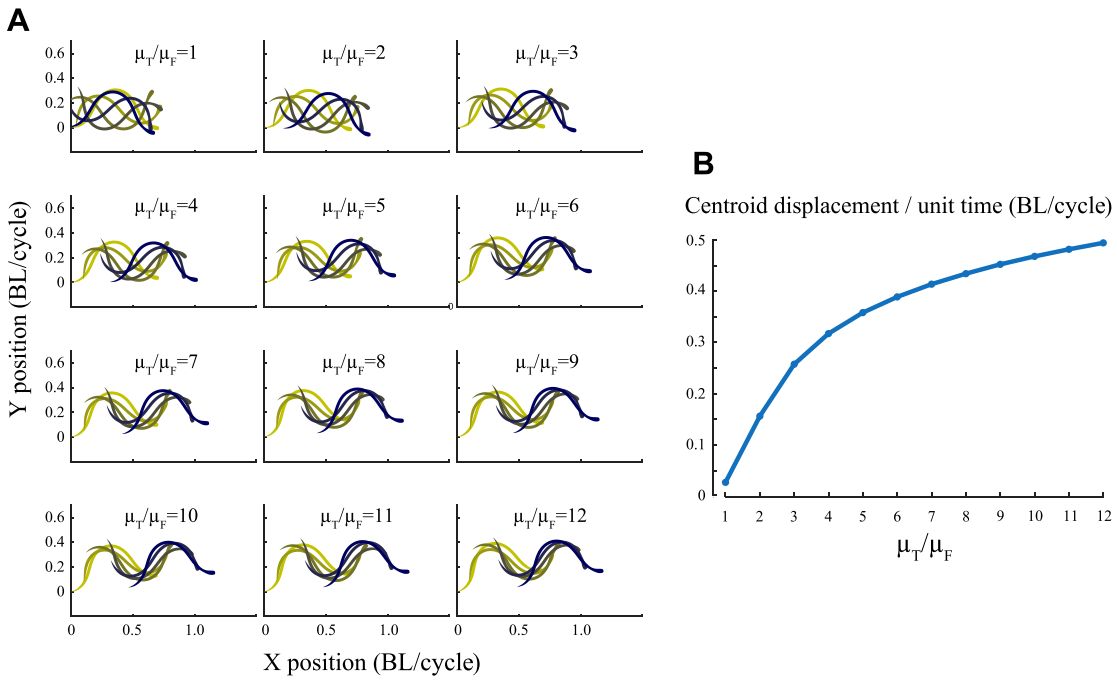


Figure 8. Results of snake locomotion simulations as a function of frictional anisotropy. A prescribed traveling-curvature wave was used to simulate planar lateral undulation under anisotropic Coulomb-like friction. Forward friction was held constant at $\mu_F = 1$ and transverse friction was varied from $\mu_T = 1$–12. Performance was quantified as centroid displacement per unit time between $t = 10$ and $t = 20$. Displacement increased with increasing anisotropy, but ratios near the experimentally measured transverse/forward friction ratios produced limited net displacement relative to simulations with substantially higher anisotropy.

locomotion in snakes. More sophisticated models that incorporate behaviors such as body lifting, rib motion, scale-catching, and normal force redistribution are needed to explain how snakes move on terrestrial and arboreal substrates.

4.4. Implications for bioinspired design

For bioinspired limbless robots and artificial skins, our results suggest four design principles. First, passive frictional anisotropy in the range measured here ($\mu_T/\mu_F \approx 1$–2) may improve locomotion but may not be sufficient by itself to reproduce robust snake-like climbing. Second, surface features should operate at multiple length scales so that the body can interact with both fine texture and larger asperities. Third, intermittent anchoring structures may be more useful on rough natural substrates than a uniformly high coefficient of friction. Finally, mechanisms that actively or passively redistribute normal force along the body may allow a robot to exploit local anchors while limiting slip elsewhere.

Acknowledgments

We thank members of the Socha Lab for assistance with animal care and discussion. We also thank Professor Tobias Seidl for supervisory support.

Data availability statement

The data that support the findings of this study are openly available at the following URL/DOI: https://github.com/TheSochaLab/Substrate-dependent-friction-and-climbing-performance-in-a-flying-snake.

Supplementary Material available at https://doi.org/10.1088/1748-3190/aebb86/data1.

Supplementary Movie 1 available at https://doi.org/10.1088/1748-3190/aebb86/data2.

Supplementary Movie 2 available at https://doi.org/10.1088/1748-3190/aebb86/data3.

Funding statement

We acknowledge the support of the National Science Foundation (1351322, 2027523).

Conflict of interest

The authors declare no competing or financial interests.

Author contributions

Jonas Scherer 0000-0002-8358-8051
Conceptualization (equal), Data curation (lead), Formal analysis (lead), Investigation (lead), Methodology (equal), Project administration (equal), Visualization (lead), Writing – original draft (lead), Writing – review & editing (equal)

Hodjat Pendar 0000-0001-8853-0062
Conceptualization (equal), Investigation (equal), Methodology (equal), Writing – review & editing (equal)

John J Socha 0000-0002-4465-1097
Conceptualization (lead), Data curation (equal), Formal analysis (equal), Funding acquisition (lead), Investigation (equal), Methodology (equal), Project administration (lead), Resources (lead), Supervision (lead), Visualization (equal), Writing – original draft (supporting), Writing – review & editing (lead)

References

Abdel-Aal H A, Vargiolu R, Zahouani H and El Mansori M 2012 Preliminary investigation of the frictional response of reptilian shed skin *Wear* **290–291** 51–60
Alben S 2013 Optimizing snake locomotion in the plane *Proc. R. Soc. A* **469** 20130236
Alben S 2019 Efficient sliding locomotion with isotropic friction *Phys. Rev. E* **99** 062402
Alben S 2022 Efficient bending and lifting patterns in snake locomotion *Proc. R. Soc. A* **478** 20220312
Alexander R M 2003 *Principles of Animal Locomotion* (Princeton University Press)
Astley H C and Jayne B C 2009 Arboreal habitat structure affects the performance and modes of locomotion of corn snakes (*Elaphe guttata*) *J. Exp. Zool. A* **311A** 207–16
Baum M J, Kovalev A E, Michels J and Gorb S N 2014 Anisotropic friction of the ventral scales in the snake *Lampropeltis getula californiae Tribol. Lett.* **54** 139–50
Berthé R A, Westhoff G, Bleckmann H and Gorb S N 2009 Surface structure and frictional properties of the skin of the Amazon tree boa *Corallus hortulanus* (Squamata, Boidae) *J. Comp. Physiol. A* **195** 311–8
Biewener A and Patek S 2018 *Animal Locomotion* (Oxford University Press)
Byrnes G and Jayne B C 2012 The effects of three-dimensional gap orientation on bridging performance and behavior of brown tree snakes (*Boiga irregularis*) *J. Exp. Biol.* **215** 2611–20
Byrnes G, Lim N T L and Spence A J 2008 Take-off and landing kinetics of a free-ranging gliding mammal, the Malayan colugo (*Galeopterus variegatus*) *Proc. R. Soc. B* **275** 1007–13
Crotty T L and Jayne B C 2015 Trade-offs between eating and moving: what happens to the locomotion of slender arboreal snakes when they eat big prey? *Biol. J. Linn. Soc.* **114** 446–58
Dellinger S B, De Vita R, Vlachos P P, Muñoz M M and Socha J J 2023 Material properties of skin in the flying snake *Chrysopelea ornata J. Exp. Zool. A* **339** 269–83
Gans C 1970 How snakes move *Sci. Am.* **223** 82–96
Graham M and Socha J J 2021 Dynamic movements facilitate extreme gap crossing in flying snakes *J. Exp. Biol.* **224** jeb242923
Graham M and Socha J J 2023 Dynamic gap crossing in *Dendrelaphis*, the sister taxon of flying snakes *J. Exp. Biol.* **226** jeb245094
Gray J 1946 The mechanism of locomotion in snakes *J. Exp. Biol.* **23** 101–20
Gray J and Lissmann H W 1950 The kinetics of locomotion of the grass-snake *J. Exp. Biol.* **26** 354–67
Hu D L, Nirody J, Scott T and Shelley M J 2009 The mechanics of slithering locomotion *Proc. Natl Acad. Sci. USA* **106** 10081–5
Jayne B C 1988 Muscular mechanisms of snake locomotion: an electromyographic study of the sidewinding and concertina modes of *Crotalus cerastes Nerodia Fasciata and Elaphe Obsoleta J. Exp. Biol.* **140** 1–33
Jayne B C 2020 What defines different modes of snake locomotion? *Integr. Comp. Biol.* **60** 156–70
Jayne B C and Davis J D 1991 Kinematics and performance capacity for the concertina locomtion of a snake (*Coluber constricter*) *J. Exp. Biol.* **156** 539–56
Jayne B C, Newman S J, Zentkovich M M and Berns H M 2015 Why arboreal snakes should not be cylindrical: body shape, incline and surface roughness have interactive effects on locomotion *J. Exp. Biol.* **218** 3978–86
Khandelwal P C, Ross S D, Dong H and Socha J J 2023 *Convergent Evolution: Animal Form and Function* ed V L Bels and A P Russell (Springer) pp 391–429
Marvi H, Cook J P, Streator J L and Hu D L 2016 Snakes move their scales to increase friction *Biotribology* **5** 52–60
Marvi H and Hu D L 2012 Friction enhancement in concertina locomotion of snakes *J. Royal. Soc. Interface* **9** 3067–80
McWhirter-Hall N A, Socha J and Khandelwal P 2026 Take-off behavior of the flying lizard *Draco dussumieri Society for Integrative and Comparative Biology* 66 (Oxford University Press) 191
Mei D, Yu X, Tang G, Kong W, Zhao X, Zhao C, Li B and Wang Y 2024 A soft crawling robot with multi-modal locomotion inspired by the movement mechanism of snake scales *IEEE Robot. Autom. Lett.* **9** 7589–96
Moon B R and Gans C 1998 Kinematics, muscular activity, and propulsion in gopher snakes *J. Exp. Biol.* **201** 2669–84
Panyutina A A, Korzun L P and Kuznetsov A N 2015 *Flight of Mammals: From Terrestrial Limbs to Wings* (Springer) pp 205–25
Rieser J M, Li T-D, Tingle J L, Goldman D I and Mendelson J R III 2021 Functional consequences of convergently evolved microscopic skin features on snake locomotion *Proc. Natl Acad. Sci. USA* **118** e2018264118
2012 *Natural Locomotion in Fluids and on Surfaces* ed S Childress *et al* (Springer) pp 117–35
Socha J J 2002 Gliding flight in the paradise tree snake *Nature* **418** 603–4
Socha J J 2006 Becoming airborne without legs: the kinematics of take-off in a flying snake, *Chrysopelea paradisi J. Exp. Biol.* **209** 3358–69
Socha J J 2011 Gliding flight in *Chrysopelea*: turning a snake into a wing *Integr. Comp. Biol.* **51** 969–82
Socha J J 2026 Substrate dependent friction and climbing performance in a flying snake *GitHub* (available at: https://github.com/TheSochaLab/Substrate-dependent-friction-and-climbing-performance-in-a-flying-snake)

Socha J J, Miklasz K, Jafari F and Vlachos P P 2010 Non-equilibrium trajectory dynamics and the kinematics of gliding in a flying snake *Bioinspir. Biomim.* **5** 045002

Socha J J, O'Dempsey T and LaBarbera M 2005 A 3-D kinematic analysis of gliding in a flying snake, *Chrysopelea paradisi J. Exp. Biol.* **208** 1817–33

Wu W, Yu S, Schreiber P, Dollmann A, Lutz C, Gomard G, Greiner C and Hölscher H 2020 Variation of the frictional anisotropy on ventral scales of snakes caused by nanoscale steps *Bioinspir. Biomim.***15** 056014

Zhang X, Naughton N, Parthasarathy T and Gazzola M 2021 Friction modulation in limbless, three-dimensional gaits and heterogeneous terrains *Nat. Commun.* **12** 6076

Supplementary Material

Supplementary Figure:

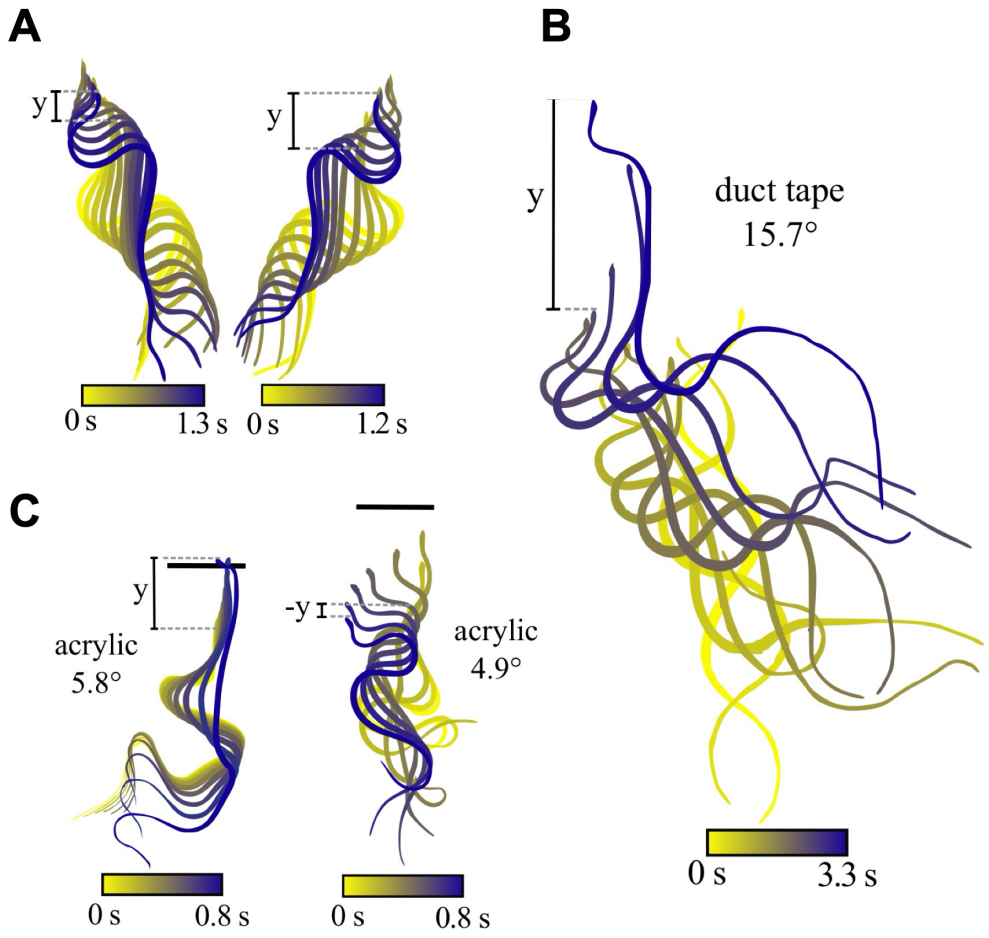


Figure S1: Additional movement patterns observed. (A) Incline climbing motion pattern of one snake (m = 56.5 g, svl = 73.5 cm). Impulsive pushes with dextral (right) and sinistral (left) body flexion are shown. (B) Straight lateral undulation and the transition to a movement with high lateral body amount of one snake (m = 74.2 g, svl = 95.9 cm). (C) 'All-or-nothing' behavior in the final phase. Snakes (left: m = 44 g, svl = 72.5 cm; right: m = 56.5 g, svl = 73.5 cm) try to reach the top edge (black bar) with one single forward strike and either succeed (left) or fail (right).

Supplementary Movie Legends

Supplementary Movie 1: Climbing movements of a representative flying snake (*Chrysopelea paradisi*) at its steepest angle on each substrate (acrylic, seam tape, duct tape, gaffer's tape, poplar bark). Snake 85's body size was mass = 44.0 g, snout-vent length (SVL) = 72.5 cm.

Supplementary Movie 2: Climbing movements of a representative flying snake (*Chrysopelea paradisi*) on one substrate (seam tape) as the incline angle increased. Snake 89's body size was mass = 56.5 g, snout-vent length (SVL) = 73.5 cm.

Supplementary Tables

Table S1: Body size data for the snakes (*Chrysopelea paradisi*) used in this study.

Snake ID	SVL (cm)	Tail length (cm)	Total length (cm)	Mass (g)
85	72.5	28.0	100.5	44.0
88	95.9	32.4	128.3	74.2
89	73.5	12.8	86.3	56.6
94	85.0	28.0	113.0	117.5
95	64.4	25.0	89.4	44.7

Table S2. Measured friction values by experiment/condition and individual animal. These values were used to calculate animal-level means for the mixed-effects analyses. Trial n is the number of trials by each individual snake to a given friction type, substrate, and direction. Animal mean μ is the mean coefficient of friction for that snake and condition. Full-slide trials on bark are not included in this table.

friction type	substrate	direction	snake ID	trial n	animal mean μ
dynamic	acrylic	backward	89	2	0.238
dynamic	acrylic	backward	94	1	0.269
dynamic	acrylic	forward	89	2	0.120
dynamic	acrylic	forward	94	1	0.185
dynamic	duct tape	backward	85	1	0.300
dynamic	duct tape	backward	88	2	0.382
dynamic	duct tape	backward	94	2	0.203
dynamic	duct tape	forward	85	1	0.188
dynamic	duct tape	forward	88	2	0.297
dynamic	duct tape	forward	94	2	0.154
dynamic	gaffer's tape	backward	85	2	0.212
dynamic	gaffer's tape	backward	88	2	0.172
dynamic	gaffer's tape	backward	94	2	0.331
dynamic	gaffer's tape	forward	85	2	0.182
dynamic	gaffer's tape	forward	88	1	0.147
dynamic	gaffer's tape	forward	94	2	0.191
dynamic	poplar bark	backward	85	3	0.348
dynamic	poplar bark	backward	88	2	0.538
dynamic	poplar bark	backward	94	4	0.543
dynamic	poplar bark	forward	88	2	0.289
dynamic	poplar bark	forward	89	2	0.280
dynamic	poplar bark	forward	94	2	0.364
dynamic	seam tape	backward	85	2	0.187
dynamic	seam tape	backward	88	2	0.226
dynamic	seam tape	backward	89	2	0.197
dynamic	seam tape	forward	85	2	0.071
dynamic	seam tape	forward	88	2	0.222
dynamic	seam tape	forward	89	2	0.051
static	acrylic	backward	89	3	0.223
static	acrylic	backward	94	3	0.277
static	acrylic	backward	95	3	0.274
static	acrylic	forward	89	3	0.185

static	acrylic	forward	94	3	0.202
static	acrylic	forward	95	3	0.210
static	acrylic	transverse	89	3	0.251
static	acrylic	transverse	94	3	0.205
static	acrylic	transverse	95	3	0.294
static	duct tape	backward	85	3	0.322
static	duct tape	backward	88	3	0.435
static	duct tape	backward	94	3	0.371
static	duct tape	forward	85	3	0.267
static	duct tape	forward	88	3	0.314
static	duct tape	forward	94	3	0.346
static	duct tape	transverse	85	3	0.390
static	duct tape	transverse	88	3	0.444
static	duct tape	transverse	94	3	0.417
static	gaffer’s tape	backward	85	3	0.482
static	gaffer’s tape	backward	88	3	0.386
static	gaffer’s tape	backward	94	3	0.362
static	gaffer’s tape	forward	85	3	0.405
static	gaffer’s tape	forward	88	3	0.256
static	gaffer’s tape	forward	94	3	0.304
static	gaffer’s tape	transverse	85	2	0.465
static	gaffer’s tape	transverse	94	3	0.366
static	poplar bark	backward	85	3	0.634
static	poplar bark	backward	88	3	0.675
static	poplar bark	backward	94	3	0.622
static	poplar bark	forward	85	4	0.342
static	poplar bark	forward	88	4	0.256
static	poplar bark	forward	89	4	0.369
static	poplar bark	forward	94	3	0.398
static	poplar bark	transverse	88	5	0.404
static	seam tape	backward	85	3	0.248
static	seam tape	backward	88	3	0.209
static	seam tape	backward	89	3	0.156
static	seam tape	forward	85	3	0.242
static	seam tape	forward	88	3	0.199
static	seam tape	forward	89	3	0.127
static	seam tape	transverse	85	3	0.302
static	seam tape	transverse	88	3	0.210
static	seam tape	transverse	89	3	0.203

Table S3. Selected coefficients and contrasts from the mixed-effects models. Log-scale estimates are shown on the model scale, with back-transformed multiplicative effects reported in the final column. Degree-scale estimates are reported in the original units. These values provide effect-size details for the model summaries in Table 5.

contrast	scale	estimaxte	SE	df	*P*	back-transformed value/units
static: seam vs acrylic	log μ	-0.14	0.09	36	0.145	0.87×
static: duct vs acrylic	log μ	0.40	0.09	36	**<0.001**	1.50×
static: gaffer vs acrylic	log μ	0.43	0.09	36	**<0.001**	1.54×
static: bark vs acrylic	log μ	0.66	0.09	36	**<0.001**	1.93×
static: forward vs backward	log μ	-0.29	0.06	36	**<0.001**	0.75×
static: transverse vs backward	log μ	-0.01	0.07	36	0.837	0.99×
dynamic: bark vs acrylic	log μ	0.62	0.21	22	**0.007**	1.87×
dynamic: forward vs backward	log μ	-0.46	0.12	22	**<0.001**	0.63×
awake slip: seam vs acrylic	log resistance	0.32	0.11	11	0.012	1.37×
awake slip: duct vs acrylic	log resistance	0.95	0.10	11	**<0.001**	2.58×
awake slip: gaffer vs acrylic	log resistance	1.22	0.10	11	**<0.001**	3.39×
max success: seam vs acrylic	degrees	5.38	2.44	15	**0.044**	+5.38°
max success: duct vs acrylic	degrees	15.89	2.44	15	**<0.001**	+15.89°
max success: gaffer vs acrylic	degrees	22.65	2.44	15	**<0.001**	+22.65°
max success: bark vs acrylic	degrees	85.06	2.44	15	**<0.001**	+85.06°
velocity: inclination slope	cm s^{-1} $degree^{-1}$	-0.44	0.07	108	**<0.001**	-0.44
head direction: inclination slope	degrees $degree^{-1}$	1.05	0.13	87	**<0.001**	1.05
centroid direction: inclination slope	degrees $degree^{-1}$	1.00	0.13	87	**<0.001**	1.00

Table S4. Data shown in Figure 5A, uphill velocity (cm/s) vs. incline angle (°). (A) Descriptive least-squares regressions of uphill velocity (cm s^{-1}) vs. platform inclination angle (°), fitted separately for each substrate, corresponding to the lines shown in Fig. 5A. Slopes are in cm s^{-1} $degree^{-1}$, intercepts are in cm s^{-1}, and *n* is the number of trials. (B) Trial counts contributed by each snake for each substrate. (C) Mixed-effects model summaries for uphill velocity, with substrate, platform inclination angle, and their interaction as fixed effects and snake ID as a random intercept. Because the substrate x platform inclination interaction was not statistically supported, the additive model was used. The high-point-excluded model represents a sensitivity analysis after excluding unusually high velocity observations identified by a median absolute deviation criterion. *P* values are from model-level *F* tests using Satterthwaite denominator degrees of freedom.

A.

substrate	slope	intercept	R2	df	P	n
acrylic	1.78	-4.55	0.13	1, 10	0.244	12
seam tape	-1.92	24.20	0.30	1, 21	0.006	23
duct tape	-0.41	12.63	0.12	1, 31	0.048	33
gaffer's tape	-0.45	14.59	0.58	1, 22	<0.001	24
poplar bark	-0.42	40.8	0.33	1, 20	0.006	22

B.

substrate	snake 85	snake 88	snake 89	snake 94	total n
acrylic	5	1	5	1	12
seam tape	7	6	4	6	23
duct tape	13	8	9	3	33
gaffer’s tape	12	6	2	4	24
poplar bark	6	5	6	5	22

C.

model type	term	df	F	*P*
full	surface	4, 102.15	6.2	**<0.001**
full	platform inclination angle	1, 101.87	0.06	0.811
full	surface × platform inclination angle	4, 102.55	1.88	0.12

additive	surface	4, 106.09	18.09	**<0.001**
additive	platform inclination angle	1, 104.96	42.66	**<0.001**
additive (high-point-excluded)	surface	4, 90.54	26.83	**<0.001**
additive (high-point-excluded)	platform inclination angle	1, 90.18	44.76	**<0.001**

Table S5. Data shown in Figure 7A, average head movement direction (°) vs. incline angle (°). (A) Descriptive least-squares regressions of average centroid movement direction (°) vs. platform inclination angle (°), fitted separately for each substrate, corresponding to the lines shown in Fig. 7B. Slopes are in degrees of movement direction per degree of platform inclination, intercepts are in degrees, and *n* is the number of trials. (B) Trial counts contributed by each snake for each substrate. (C) Mixed-effects model summaries for centroid movement direction, with substrate, platform inclination angle, and their interaction as fixed effects and snake ID as a random intercept. Bark was excluded because centroid position could not be tracked reliably against the bark substrate. Because the substrate x platform inclination interaction was not statistically supported, the additive model was used. *P* values are from model-level *F* tests using Satterthwaite denominator degrees of freedom..

A.

substrate	slope	intercept	R2	df	p	n
acrylic	1.7	18.94	0.08	1, 10	0.363	12
seam tape	2.01	7.32	0.56	1, 21	<0.001	23
duct tape	0.91	9.23	0.36	1, 31	<0.001	33
gaffer's tape	0.93	0.72	0.69	1, 22	<0.001	24

B.

substrate	snake 85	snake 88	snake 89	snake 94	total n
acrylic	5	1	5	1	12
seam tape	7	6	4	6	23
duct tape	13	8	9	3	33
gaffer’s tape	12	6	2	4	24

C.

model type	term	df	F	*P*
full	surface	3, 84	1.3	0.281
full	platform inclination angle	1, 84	0.65	0.421
full	surface × platform inclination angle	3, 84	2.84	**0.043**

Table S6. Regression statistics for lines shown in Figure 7B, average centroid movement direction (°) vs. incline angle (°). (A) Descriptive least-squares regressions of average centroid movement direction (°) vs. platform inclination angle (°), fitted separately for each substrate and corresponding to the lines shown in Fig. 7B. Slopes are in degrees of movement direction per degree of platform inclination, intercepts are in degrees, and *n* is the number of trials. (B) Trial counts contributed by each snake for each substrate. (C) Mixed-effects model summaries for centroid movement direction, with substrate, platform inclination angle, and their interaction as fixed effects and snake ID as a random intercept. Bark was excluded because centroid position could not be tracked reliably against the bark substrate. Because the substrate x platform inclination interaction was not statistically supported, the additive model was used. *P* values are from model-level *F* tests using Satterthwaite denominator degrees of freedom.

A.

substrate	slope	intercept	R2	df	p	n
acrylic	-0.61	32	0.01	1, 10	0.786	12
seam tape	1.26	14.63	0.31	1, 21	0.006	23
duct tape	0.78	9.52	0.29	1, 31	0.001	33
gaffer's tape	0.94	-3.12	0.49	1, 22	<0.001	24

B.

substrate	snake 85	snake 88	snake 89	snake 94	total n
acrylic	5	1	5	1	12
seam tape	7	6	4	6	23
duct tape	13	8	9	3	33
gaffer’s tape	12	6	2	4	24

C.

model type	term	df	F	*P*
full	surface	3, 82.70	5.85	**0.001**
full	platform inclination angle	1, 82.26	0.13	0.723
full	surface × platform inclination angle	3, 82.83	0.91	0.442
additive	surface	3, 85.18	25.94	**<0.001**
additive	platform inclination angle	1, 85.48	57.66	**<0.001**